tion in estrogen and progesterone levels. Additionally, insulin resistance in PCOS patients may lead to metabolic disorders and high oxidative stress (Murri et al., 2013; Liu et al., 2019). These findings point to a role for oxidative stress in PCOS pathogenesis.

The lipid peroxidation process central to ferroptosis can be initiated and exacerbated by oxidative stress. Excessive oxidative stress has the potential to cause elevated levels of lipid peroxides, thus facilitating ferroptotic demise (Park et al., 2021). The occurrence of ferroptosis is triggered by the buildup of lipid peroxides in an iron-reliant fashion, rendering it distinct from alternative types of controlled cellular demise(Dixon et al., 2014). Glutathione peroxidase (GPX4) plays a pivotal roles in regulating ferroptotic cell death (Dixon et al., 2012; Liu et al., 2023). Primarily, the overexpression of cyclooxygenase-2 (COX2), increase in malondialdehyde (MDA) levels, and reduction in glutathione function as pivotal markers signifying ferroptosis. These markers are critical indicators of the advancement and progression of ferroptotic cell death (Gao et al., 2015). Lipids, specifically polyunsaturated fatty acids, are susceptible to oxidative and play a vital role in ferroptosis (Xu et al., 2022). Ferroptosis is associated with various physiological and pathological mechanisms, including damage caused by ischemia–reperfusion, neurodegenerative ailments, and cancer (Stockwell et al., 2017). Numerous k

lished, seven rats were randomly assigned to either the PCOS group or the baicalein group. After treatment for 21 days, the rats in the PCOS group were treated with 0.2 ml of 0.5 % —CMC-Na, whereas those in the baicalein group were administered 25 mg/kg, 50 mg/kg or 100 mg/kg baicalein (baicalein was dissolved in 0.2 ml of 0.5 % —CMC-Na, the concentration of which was 1 μg/μl) via intraperitoneal injection for 28 days. Pregnancy was established by pairing proestrus female rats with fertile male rats of the same strain at a 2:1 ratio. Successful mating was confirmed by the presence of a vaginal plug the following morning, which was considered gestational day 0.5. On gestational day 15.5, all rats were killed, and serum samples and the ovaries, uterus, and placenta were collected. These specimens were subsequently either fixed for morphological and immunohistochemical analyses or promptly frozen in liquid nitrogen and stored at –80 ˚C for Western blot analysis and RNA sequencing.

Hematoxylin and eosin staining

The ovarian and placental tissues of the rats were immediately fixed in 4 % paraformaldehyde (BL539A, Biosharp, Beijing, China). After paraffin embedding, the tissues were cut into 4 μm slices. Next, the tissue sections were immersed in a hematoxylin solution, which selectively stains the nuclei a blue–purple color. After staining, the tissue was differentiated in an acid alcohol solution to remove excess stain and achieve the desired contrast between the nuclei and other tissue components. To enhance the color and contrast of the hematoxylin-stained nuclei, the tissue sections were briefly exposed to a weak alkaline solution, such as running tap water, in a process called “bluing”. Following bluing, the tissue underwent eosin staining, which imparted a pink color to the cytoplasm and other extracellular components. This step is relatively short compared to hematoxylin staining. After staining, the tissue sections were dehydrated using a series of alcohol baths of increasing concentration to remove water. Then, the slides were cleared in xylene to prepare for mounting. Finally, the tissue sections were mounted on a slide with a coverslip using a mounting medium. Finally, the ovarian and placental tissues were prepared for microscopic examination (EVOS M7000, Thermo Fisher Scientific, Waltham, USA). This procedure allowed the visualization of tissue structures; the cell nuclei appeared blue, which facilitated the histological analysis of the ovarian and placental tissues.

Perls’ histochemical reaction

Iron deposition in the placenta was evaluated by diaminobenzidine (DAB)-enhanced Perls’ staining. Following deparaffinization and rehydration, the tissue sections were submerged in a mixture of equal volumes of potassium ferrocyanide solution and hydrochloric acid solution for 1 h at room temperature. The sections were rinsed with PBS five times for 5 min each, exposed to DAB for 10 min , and finally treated with pararosaniline solution for 2 min . Images of the distribution of iron were taken using a microscope (EVOS M7000, Thermo Fisher Scientific, Waltham, USA).

Immunohistochemistry of placental tissue

The tissues were fixed for 24 h in 4 % paraformaldehyde at 4 ˚C, embedded in paraffin, and subsequently sectioned into slices with a thickness of 4 μm. Next, the tissues were blocked in a 0.5 % bovine serum albumin solution and incubated with primary antibodies against FTH1 (1:200) and COX2 (1:200) overnight. Next, the sections were incubated with biotin-conjugated secondary antibodies (1:300) for 1 h at 25 ˚C for visualization. The coverslips were counterstained using hematoxylin and eosin for 5 min at 25 ˚C. Finally, the samples were examined under a fluorescence microscope (EVOS M7000, Thermo Fisher Scientific, Waltham, USA).

Transmission electron microscopy

The KGN cell pellets and ovarian tissue were fixed with 2.5 % glutaraldehyde at room temperature. The plates were incubated first for 2 h and then for 24 h (overnight) at 4 ˚C. The following day, the KGN cells and ovarian tissue were dehydrated with ethanol and cut into 100 nm sections. Next, the sections were treated with uranyl acetate and lead citrate. Finally, the sections were analyzed via transmission electron microscopy (Leica, Weztlar, Germany).

JC-1 staining

JC-1 is an effective fluorescent probe that is extensively utilized for detecting the mitochondrial membrane potential (MMP). The cells treated with the drug were stained with JC-1 working solution for 20 min , followed by two washes with the prepared JC-1 staining buffer. Subsequently, 2 ml of cell culture medium was added, and the cells were observed under a laser confocal microscope (Olympus, Japan). The fluorescence intensity ratio of green to red was used to indicate the MMP.

ROS staining

The cell fluorescence probe 2′,7′-dichlorodihydrofluorescein diacetate was used to determine oxidative stress. We used this method to assess the intracellular ROS levels in KGN cells. Dichlorodihydrofluorescein diacetate working solution was added to the DHEA-treated cells, which were subsequently incubated at 37 ˚C for 30 min. The cells were subsequently washed with a serum-free culture medium. Subsequently, the fluorescence signal of dichlorofluorescein was measured using a fluorescence microscope, which reflects the intracellular ROS levels.

Dihydroethidium is a probe that can enter cells freely and be oxidized by ROS to form oxyethidium. This product binds to DNA and generates a red fluorescent signal. The intensity of the red fluorescence detected in living cells was used to determine the level of ROS and changes in the cells. Frozen tissue sections of the rat placenta were placed in DHE working solution. The sections were fully immersed in a staining solution to allow DHE to penetrate the tissue. These sections were incubated at 37 ˚C for 30 min and then washed with PBS to remove any unabsorbed DHE and dimethyl sulfoxide (DMSO). Finally, the sections were observed, and images were collected under a Nikon fluorescence microscope.

Iron assay

Levels of ferrous iron were quantified by means of an iron assay kit. First, a 10 μl aliquot from the 100 mM standard solution was diluted, and a 1 mM standard solution (0, 2, 4, 6, 8, and 10 μl) was introduced into a 96-well plate to create standards with concentrations of 0, 2, 4, 6, 8, and 10 nmol/well per well. Iron assay buffer was added to each well, and the volume was 100 μl. Next, 5 μl of iron reducer was added to each standard well. The tissues and cells were swiftly homogenized in 4–10 vol of iron assay buffer. Subsequently, the samples were centrifuged at 16, 000 × *g* for 10 min at 4 ˚C to eliminate insoluble material. Subsequently, the samples were dispensed into 96-well plates. After incubating at 37 ˚C for 1 hour, the absorbance was measured at 593 nm using an automatic microplate reader (Promega, Madison, USA).

Detection of ROS, SOD, MDA, and GSH

Blood samples from the rats were subjected to centrifugation at 3000 rpm for 15 min for biochemical analysis. The levels of ROS, SOD, MDA, and GSH were subsequently determined using the corresponding assay kits following the manufacturer's instructions. The tissues or cells were homogenized with PBS. Following homogenization or lysis, the

samples were centrifuged at 10, 000 × *g* - 12, 000 × *g* for 10 min , after which the resulting supernatant was collected for subsequent analysis. We determined the protein concentration of tissue or cell samples after preparation with a BCA protein concentration determination kit. Using this method, we calculated the protein content in tissue or cells per unit protein weight. The optical density was quantified at 450 nm using an automatic microplate reader (Promega, Madison, USA).

ELISA

We performed IL-6, IL-18, and TNF-α assays using suitable kits. A blank control hole and standard holes were set; then, 50 μl of serum was directly added to test each test well. Next, 50 μl of enzyme-labeled antigens and antibodies were added to all the wells, the contents were thoroughly mixed, the sealing plate mold was added, and the mixture was incubated at 37 ˚C for 1 hour. Then, the plate was washed manually, developer A and developer B were added to each well, and the treated samples were incubated at 37 ˚C for 15 min . Finally, a termination solution was added, and the optical density was quantified at 450 nm using an automatic microplate reader (Promega, Madison, USA).

Western blot

Protein extraction was carried out by lysing tissues or cells in RIPA buffer which was supplemented with protease and phosphatase inhibitors. To determine protein concentrations, BCA assays were conducted. Equal amounts of proteins were then loaded onto sodium dodecyl sulfate

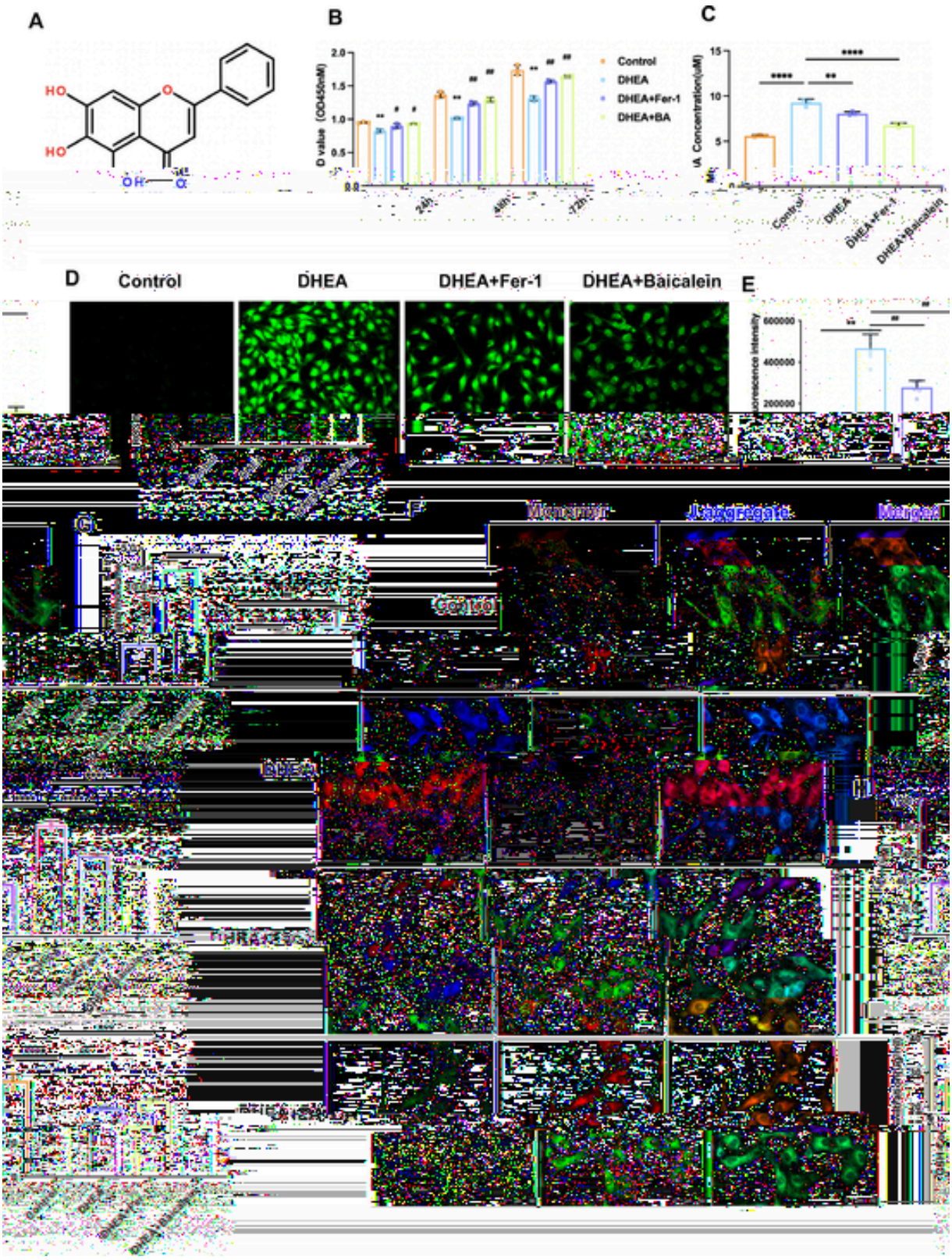

Fig. 1. Baicalein restores DHEA-induced lipid peroxidation in KGN cells

KGN cells were treated with Fer-1 (10 μmol/l) or baicalein (20 μmol/l) for 5 h, and DHEA (20 μmol/l) was used to stimulate KGN cells for 24 h, 48 h, or 72 h. In all plots, the values are expressed as the means ± SEMs. The p values for selected comparisons are indicated as * $p < 0.05$, # $p < 0.05$, * *$p < 0.01$, # #$p < 0.01$, ***$p < 0.001$, and ****$p < 0.0001$. A. Chemical structure of baicalein. B. Cell viability was measured at an OD of 450 nm after culture for different durations. C. The level of MDA activity in KGN cells was determined. D-E. ROS distribution and fluorescence intensity were determined via laser confocal

Fig. 1.—*continued*
imaging. F-G. Changes in the MMP of KGN cells were detected via laser confocal microscopy. H. The level of Fe^{2+} was assessed using an iron reagent test kit. I. The level of GSH activity in KGN cells was determined.

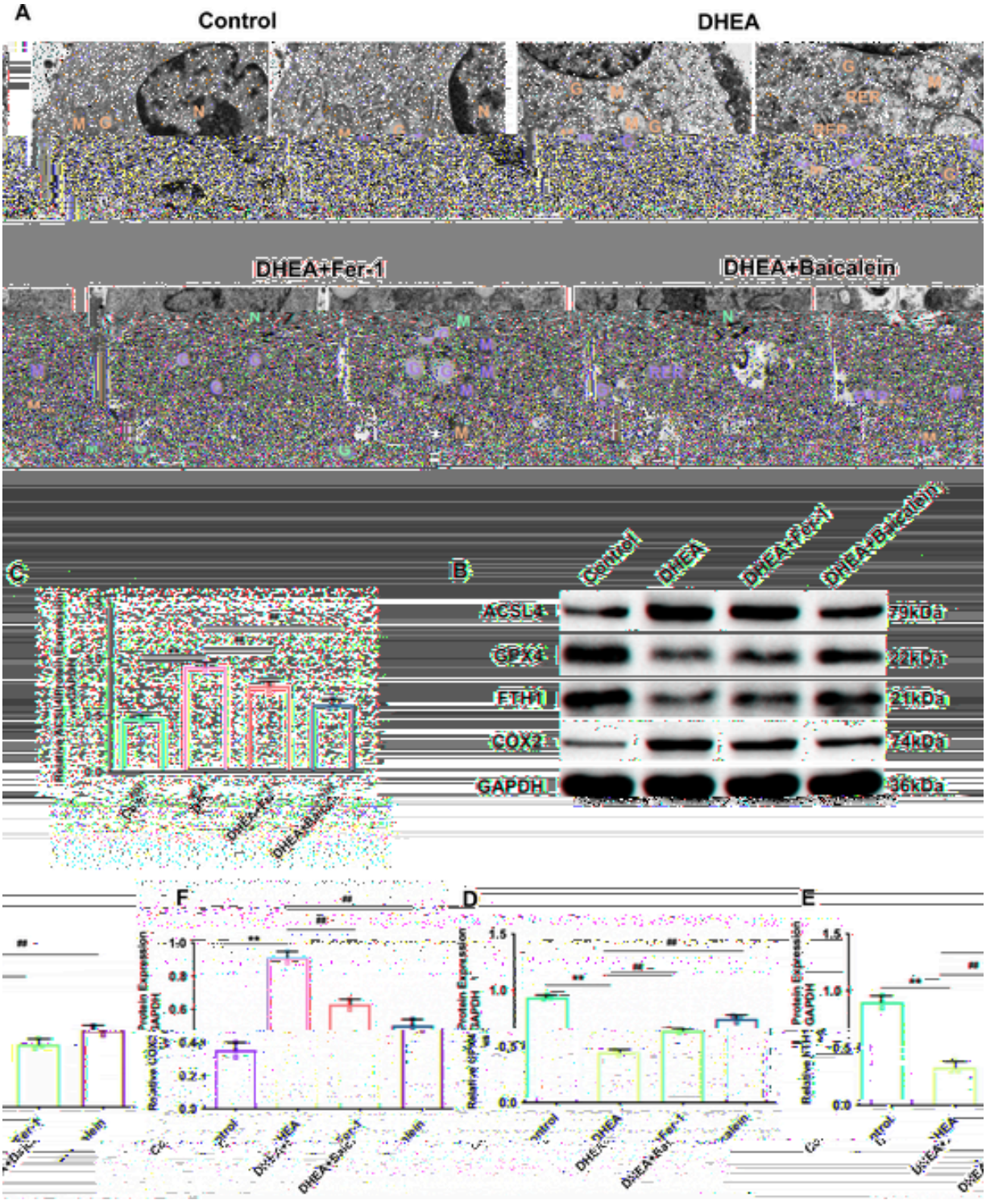

Fig. 2. Baicalein reduces DHEA-induced KGN cell ferroptosis
The KGN cells were cultivated and grouped into control, DHEA, DHEA + Fer-1, and DHEA + baicalein groups. In all plots, the values are expressed as the mean ±SEM. The p values for selected comparisons are indicated as * $^{*}p < 0.01$, and # $^{\#}p < 0.01$. A. Images of KGN cell morphology and mitochondrial morphology were observed under an electron microscope. B-F. The protein levels of ACSL4, GPX4, FTH1, and COX2 in KGN cells.

ferent groups of KGN cells. These findings showed a marked decrease in expressing GPX4 and FTH1 upon stimulation with DHEA. Concurrently, there was an upregulation of ACSL4 and COX2 expression. However, following treatment with Fer-1 or baicalein, GPX4 and FTH1 protein significantly increased, ACSL4 and COX2 expression decreased (Fig. 2B-F).

Based on the above findings, we inferred that when KGN cells were exposed to DHEA, ferroptosis increased significantly. However, treatment with Fer-1 or baicalein effectively decreased ferroptosis in KGN cells.

Baicalein alleviated ovarian dysfunction in DHEA-induced PCOS rats

Fig. 3A outlines the experimental procedures. The rats were injected with sesame oil as a sham control. Rats were randomly assigned to six groups: the oil + 0.5 % —CMC-Na group, DHEA + 0.5 % —CMC-Na group, DHEA + Fer-1 group, DHEA + baicalein (25 mg/kg) group, DHEA + baicalein (50 mg/kg) group, and DHEA + baicalein (100 mg/kg) group. At the conclusion of the present study, the PCOS group demonstrated a significantly greater rat weight than the control group. Fer-1 or baicalein at 100 mg/kg reduced the weight of the PCOS rats(Fig.3C). Subsequently, alterations in ovarian pathology were assessed among the different groups(Fig.3B). We also measured luteinizing hormone (LH), E2, and testosterone (T) levels. Some research have showed that baicalein can inhibit ovarian cancer, while no studies explored the effects of baicalein on PCOS (Chuang et al., 2023). Our data showed that serum sex hormone levels were significantly higher in PCOS rats after treatment with baicalein (Fig. 3D-G). Overall, Fer-1 and 100 mg/kg baicalein had promising effects on mitigating histological changes and improving ovarian function.

Baicalein attenuated lipid peroxidation and chronic inflammation in DHEA-induced PCOS rats

Baicalein has known anti-inflammatory and anti-oxidative stress properties. It is reported that can be used to treat osteoarthritis(Wan et al., 2023). For evaluation of the impact of baicalein on oxidative stress, we examined the serum and ovarian tissue levels of oxidative stress markers and antioxidant substances. Compared with control rats, PCOS rats exhibited significantly greater serum ROS and MDA levels but lower serum SOD and GSH levels. After Fer-1 intervention, the levels of ROS and MDA decreased significantly, while SOD and GSH levels did not change. Administering baicalein at 100 mg/kg significantly decreased the serum ROS and MDA levels and increased the serum SOD and GSH levels (Fig. 4A–I). Next, we measured the inflammatory factor levels in the serum and found that 100 mg/kg baicalein significantly decreased the IL-18, IL-6, and TNF-α levels (Fig. 4J–L). These findings suggested that in PCOS rats, lipid peroxidation and inflammation increase. However, these effects diminished following baicalein treatment.

Baicalein mitigated ovarian ferroptosis in DHEA-induced PCOS rats

Increased iron accumulation and lipid peroxidation have been shown in PCOS rats (Macut et al., 2013). We investigated the key regulatory molecules of ferroptosis in the ovary via Western blotting analysis and assessed morphological changes in ovarian granulosa cells through transmission electron microscopy. The results indicated that rats with PCOS exhibited reduced expression of GPX4 and FTH1, elevated expression of ACSL4 and COX2, fewer mitochondrial cristae, and greater membrane density; these changes indicated ferroptosis and mitochondrial dysfunction. However, treatment with Fer-1 and baicalin at 100 mg/kg partially inhibited ferroptosis (Fig. 5A, B). These findings suggest that appropriate doses of baicalein may have beneficial effects on ferroptosis and mitochondrial dysfunction in PCOS rats.

Genes associated with ferroptosis are altered in the placenta

To assess whether baicalein impacts pregnancy outcomes in patients with PCOS, we established a pregnant rat model of PCOS. This choice was made because PCOS can substantially affect the reproductive capabilities of women of childbearing age. The experimental processes are illustrated in Fig. 6A. RNA sequencing of placental tissue from the three groups of rats revealed that the gene expression differed significantly among the placental tissues (Fig. 6B, C). The results of the gene enrichment analysis were visualized using GO and KEGG pathway diagrams. The results indicated that the signaling pathways were associated with the cell cycle, iron ion transport, reactive oxygen species metabolism, and the insulin response (Fig. 6D, E). According to the FerrDb database, ferroptosis-related genes were classified into two categories: ferroptosis-positive regulatory signatures, which promote ferroptosis, and ferroptosis-negative regulatory signatures, which suppress ferroptosis. Furthermore, we compared the transcriptome sequences of rat placental tissue and the genes listed in the FerrDb database to identify the common genes found in both datasets. The occurrence of ferroptosis was more intense in the placental tissues of PCOS rats, and this change was subsequently alleviated by administering baicalein.

Baicalein ameliorated placental development in DHEA-induced PCOS gravid rats

FTH1 can protect cells against ferroptosis by sequestering excess intracellular iron, thus preventing its involvement in iron-dependent lipid peroxidation reactions (Mi et al., 2023; Zhang et al., 2021). Several studies have reported that COX2 might play a protective role in ferroptosis by promoting anti-inflammatory and cytoprotective effects, while others have suggested that COX2 can contribute to ferroptosis by facilitating lipid peroxidation and oxidative stress (Kohandel et al., 2021; Wang et al., 2022). Based on the results of the sequencing analysis, we performed immunohistochemistry (IHC) on rat placental tissues to assess the expression of ferroptosis regulatory molecules, specifically FTH1 and COX2. The results of the analysis confirmed the patterns observed in the sequencing data (as shown in Fig. 7A, B). We also investigated the changes in ferroptosis-related molecules in the ovaries, placenta, and uterus in each experimental group. The results indicated a significant decrease in GPX4 expression in the PCOS group, whereas the expression of ACSL4 substantially increased. After treatment with baicalein, the expression of the GPX4 protein increased significantly, but the expression of ACSL4 decreased significantly (Fig. 7C–E). As shown in Fig. 7F, placental ROS levels in the PCOS group were considerably greater than those in the control group. However, after administering baicalein, ROS production decreased significantly in placental tissue. Next, we conducted prussian blue staining to visualize iron deposits in ovarian and placental tissues and investigate the occurrence of ferroptosis. Our results indicated that iron deposition in the PCOS group was greater than that in the control group, and baicalein reversed these changes. Iron deposition may contribute to the initiation and progression of ferroptosis in placental tissues, and baicalein may have therapeutic effects by reducing iron deposition and inhibiting ferroptosis (Fig. 7G, H). These findings indicated that baicalein might ameliorate gravid placental development by mitigating ferroptosis.

Discussion

In this study, we presented two new findings. First, PCOS is correlated with oxidative stress, ferroptosis, and chronic inflammation.

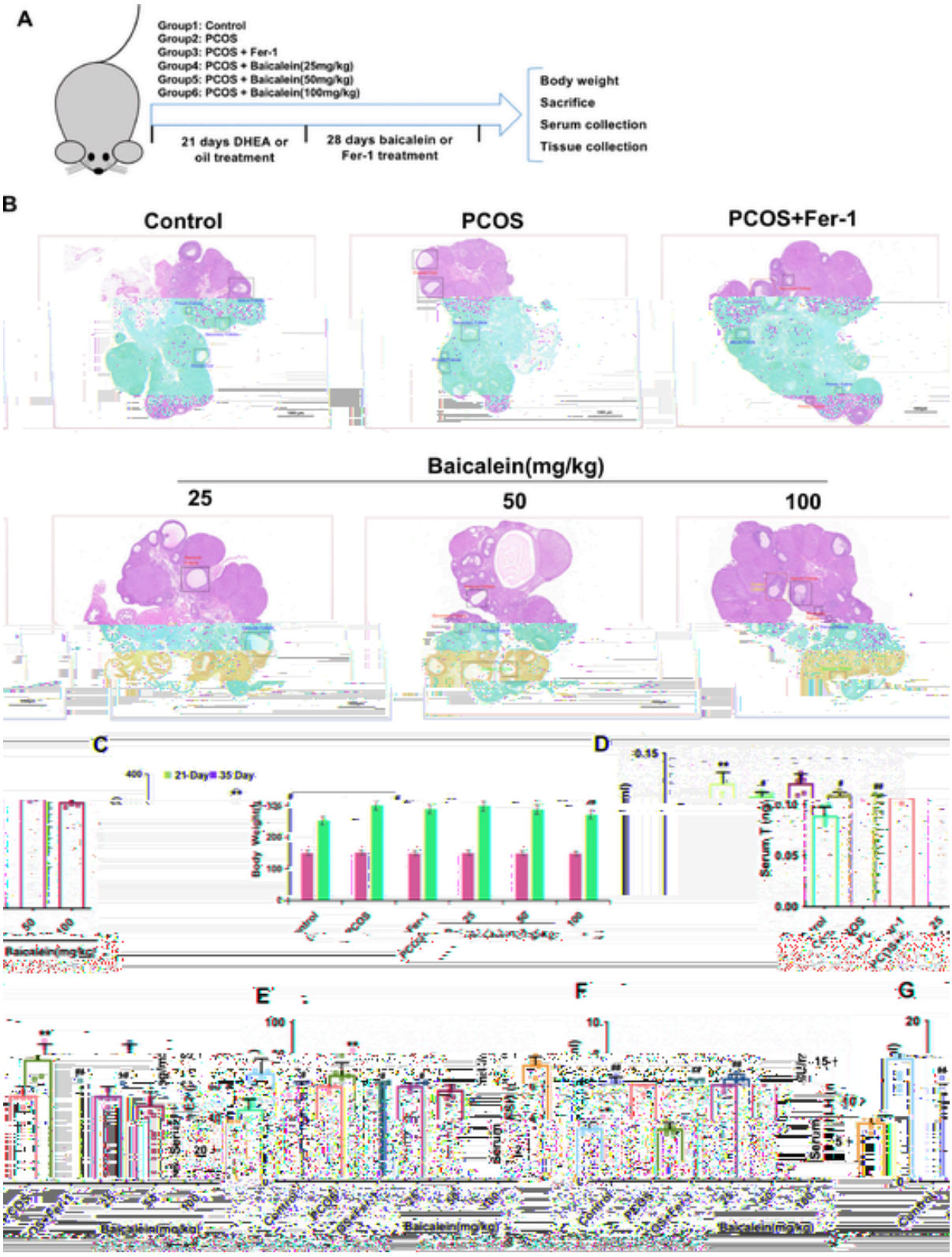

Fig. 3. Baicalein alleviated ovarian dysfunction in DHEA-induced PCOS rats

In all plots, the values are expressed as the means ±SEMs. The p values for selected comparisons are indicated as * $p < 0.05$, # $p < 0.05$, * *$p < 0.01$, and # #$p < 0.01$.A. The experimental processes are illustrated. Since DHEA was dissolved in sesame oil during the experiment, the sesame oil-treated group was used as a sham control. The rats were randomly divided into six groups: the oil + 0.5 % —CMC-Na, DHEA + 0.5 % —CMC-Na, DHEA + Fer-1, DHEA + baicalein (25 mg/kg), DHEA + baicalein (50 mg/kg) and DHEA + baicalein (100 mg/kg) groups. The rats were weighed on days 21 and 35. Each

Fig. 3.—*continued*
group included seven rats (n = 7). B. The ovaries were stained with H&E. C. The rats were weighed on days 21 and 35. D. Serum T levels in each group. E. Serum E2 levels in each group. F. Serum FSH levels in each group. G. Serum LH levels in each group.

Second, baicalein effectively attenuated DHEA-induced ovarian dysfunction and gravid placental development in rats with PCOS (Fig. 8).

PCOS, a prevalent metabolic disorder marked by metabolic issues, such as hyperandrogenaemia, chronic inflammation, and oxidative stress. These factors can also disrupt ovulation and impair the functions of ovaries (Escobar-Morreale, 2018). Clinically, as the etiology and pathogenesis of PCOS remain unknown, the main treatment administered is symptomatic relief (Kauffman et al., 2015). Baicalein has antibacterial, diuretic, anti-inflammatory, antiallergic, and spasmolytic effects (Liao et al., 2021; Palierse et al., 2021; Yarla et al., 2016). Baicalein is an effective component in the body and can quickly be converted into baicalin and other metabolites in the blood (Pan et al., 2021; Banik et al., 2022; Chuang et al., 2023). The role of baicalein in ferroptosis related to tumors, sepsis, and hypoxic kidney injury was investigated, and baicalein was found to be a promising therapeutic agent for reducing ferroptosis-related tissue damage (Kong et al., 2021; Wan et al., 2023). However, research examining the direct impact of baicalein on PCOS is scarce. This objective of this study were investigating the influence of baicalein on ovarian function. Our study delineates the novel therapeutic potential of baicalein in addressing both metabolic disorders and inflammatory responses, establishing a significant breakthrough in the field. Our results revealed a compelling correlation between baicalein administration and the amelioration of metabolic irregularities, as evidenced by the substantial improvement in body weight dynamics and the notable reduction in inflammatory cytokine levels in rats with PCOS. This dual-action effect of baicalein presents a pioneering avenue for addressing multifaceted aspects of PCOS-related pathophysiology. Moreover, our investigation reveals the unprecedented efficacy of baicalein in mitigating ovarian dysfunction and effectively countering the pathological damage observed in the ovarian tissues of PCOS-afflicted rats. This nuanced insight underscores the innovative potential of baicalein as a therapeutic agent with a comprehensive impact on both systemic metabolic health and specific ovarian functionality in the context of PCOS. However, additional research is needed into the mechanism of action of this drug, which is the subject of this report.

Approximately half of the patients with PCOS are obese, and they have high total free fatty acids, including arachidonic acid, which can alter the cellular mitochondrial distribution and increase ROS production (Ma et al., 2022; Lin et al., 2020). A notable increase in markers of the oxidative cycle is regarded as a potential initiator of the pathogenesis of PCOS (Mohammadi, 2019). In the metabolic process, oxygen-free radical reactions and lipid peroxidation reactions play crucial roles. Under normal circumstances, they exist in a well-coordinated and dynamic equilibrium, contributing to several physiological, biochemical, and immune responses (Zhang et al., 2021). During lipid peroxidation, ROS oxidize the components of biomembranes, including the side chains of nucleic acids, polyunsaturated fatty acids and other macromolecules associated with ROS and phospholipids. Membrane receptors and enzymes in the biomembrane are affected by lipid peroxidation, which leads to the formation of lipid peroxidation products such as MDA and 4-hydroxynonenoic acid. These changes, in turn, alter the permeability and fluidity of the cell membrane, ultimately resulting in changes in the structure and function of cells (Jelinek et al., 2022; Li et al., 2022; Ma et al., 2022).

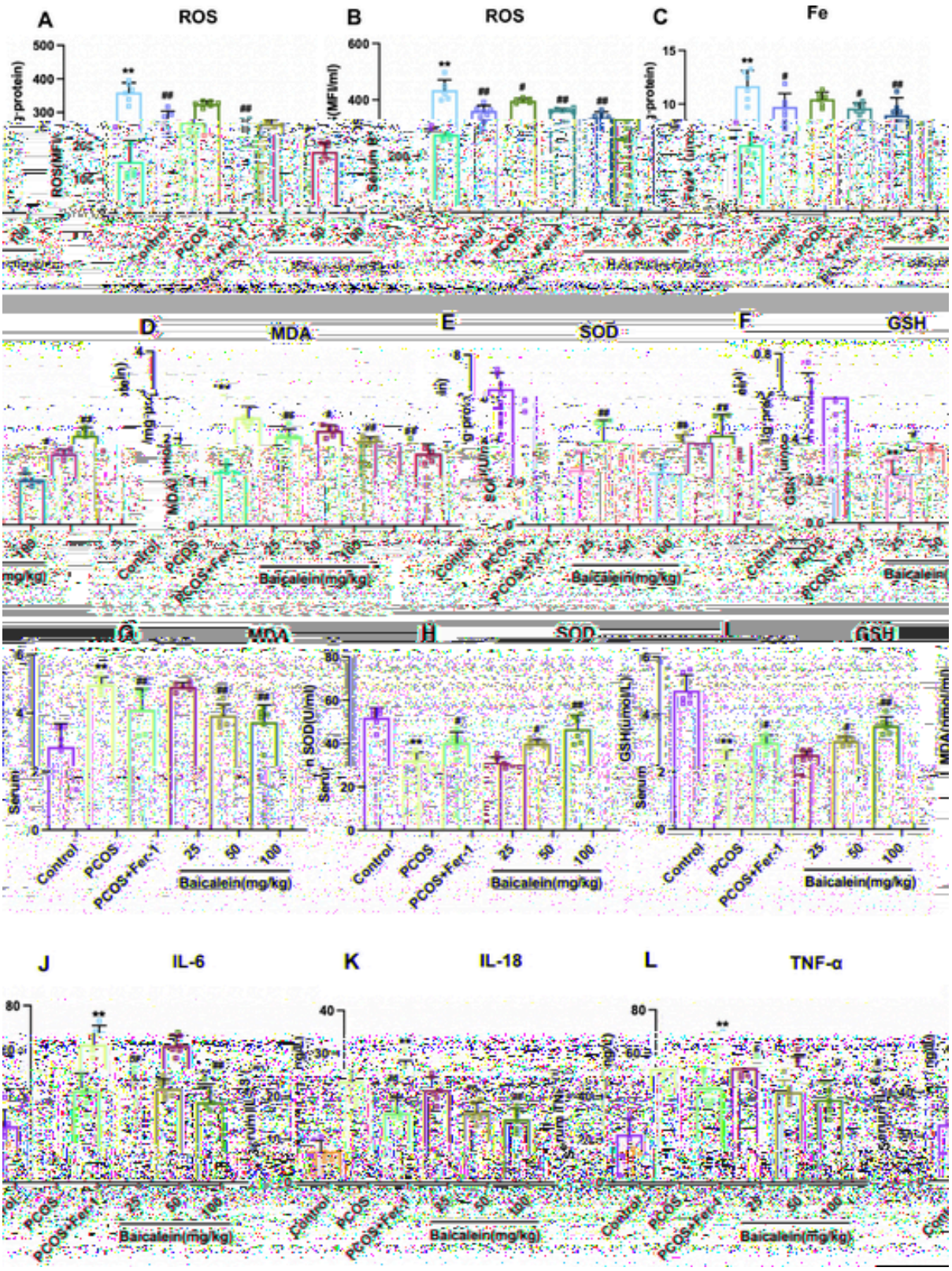

Fig. 4. Baicalein attenuated lipid peroxidation and chronic inflammation in DHEA-induced PCOS rats
In all plots, the values are expressed as the

Fig. 4.—*continued*
tration in the different groups was determined via ELISA. H. The serum SOD concentration in the different groups was determined via ELISA. I. The serum GSH concentration in the different groups was determined via ELISA. J. The serum IL-6 concentration in the different groups was determined via ELISA. K. The serum IL-18 concentration in the different groups was determined via ELISA. L. The TNF-α concentration in the serum of the different groups was determined
vi

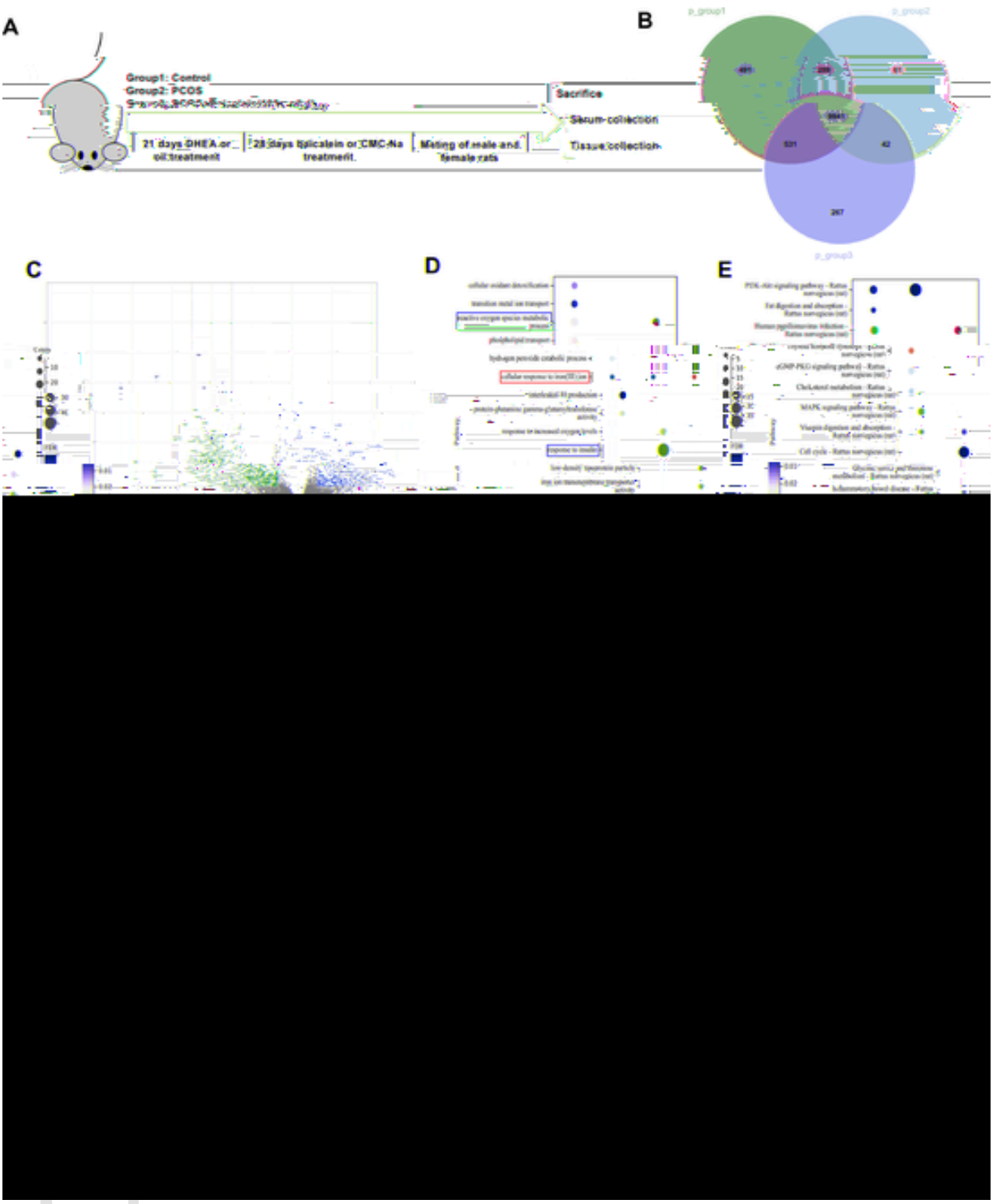

Fig. 6. Genes associated with ferroptosis are altered in the placenta
A. The experimen

types of cells, each of which has a different gene/protein expression pattern that may be sensitive to baicalein treatment. Ferroptosis pathways in isolated placental regions or isolated cell types in baicalein-treated rat placentas should also be analyzed in future studies.

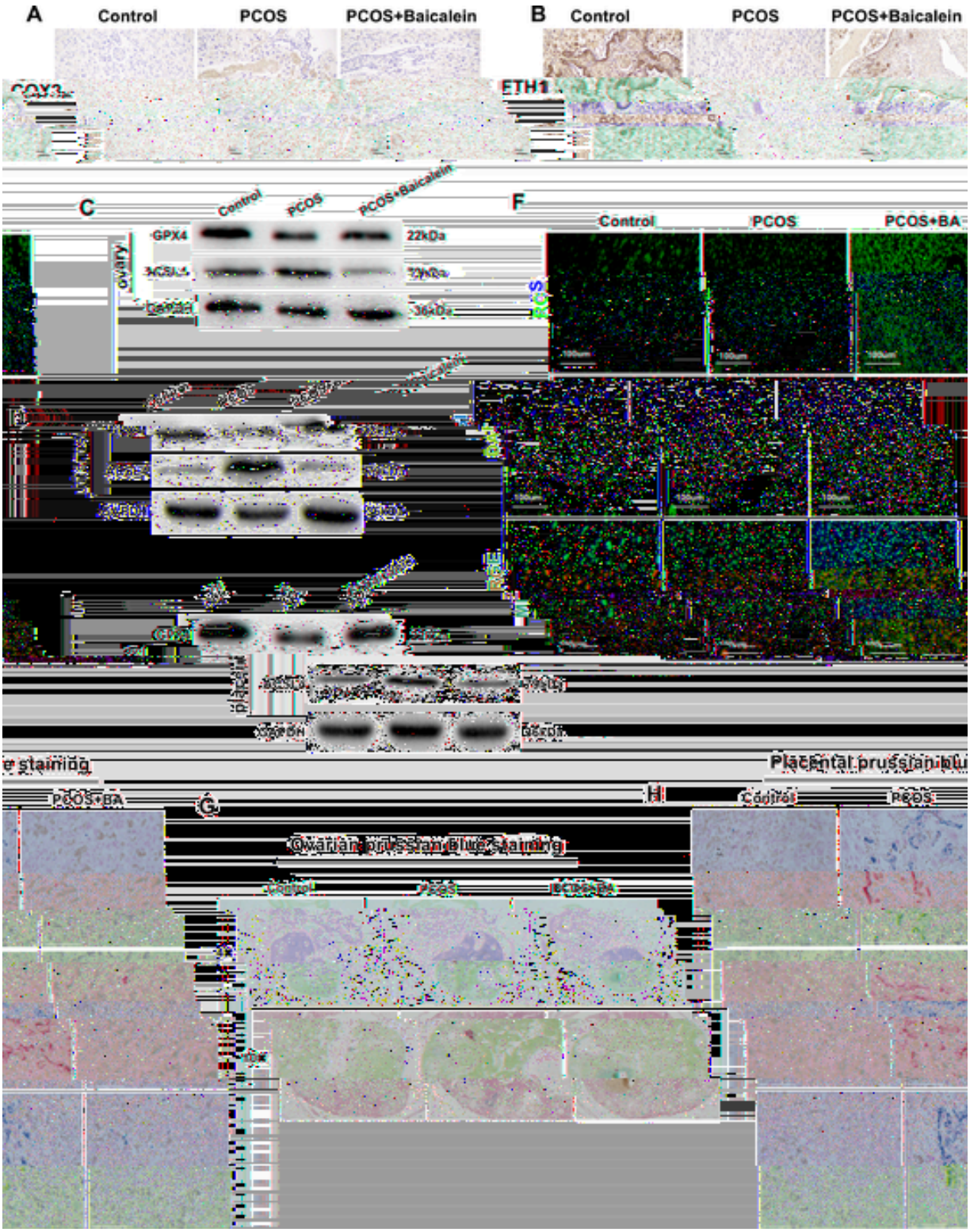

Fig. 7. Baicalein ameliorated placental development in DHEA-induced PCOS gravid rats
A. The expression of COX2 in the placental tissue of rats was evaluated by immunohistochemistry. B. The expression of FTH1 in the placental tissue of rats was determined by immunohistochemistry. C. GPX4 and ACSL4 protein levels in ovarian tissue were assessed via Western blotting. D. GPX4 and ACSL4 protein levels in the uterine tissue of rats were assessed via Western blotting. E. The expression of GPX4 and ACSL4 in the placental tissue of rats was evaluated by Western blotting. F. The level of ROS in the placenta of the rats in the three groups was determined using a fluorescence microscope. G. Iron deposition in the placenta was detected by DAB-enhanced Perls' staining. H. Iron deposition in the gravid placenta was detected by DAB-enhanced Perls' staining.

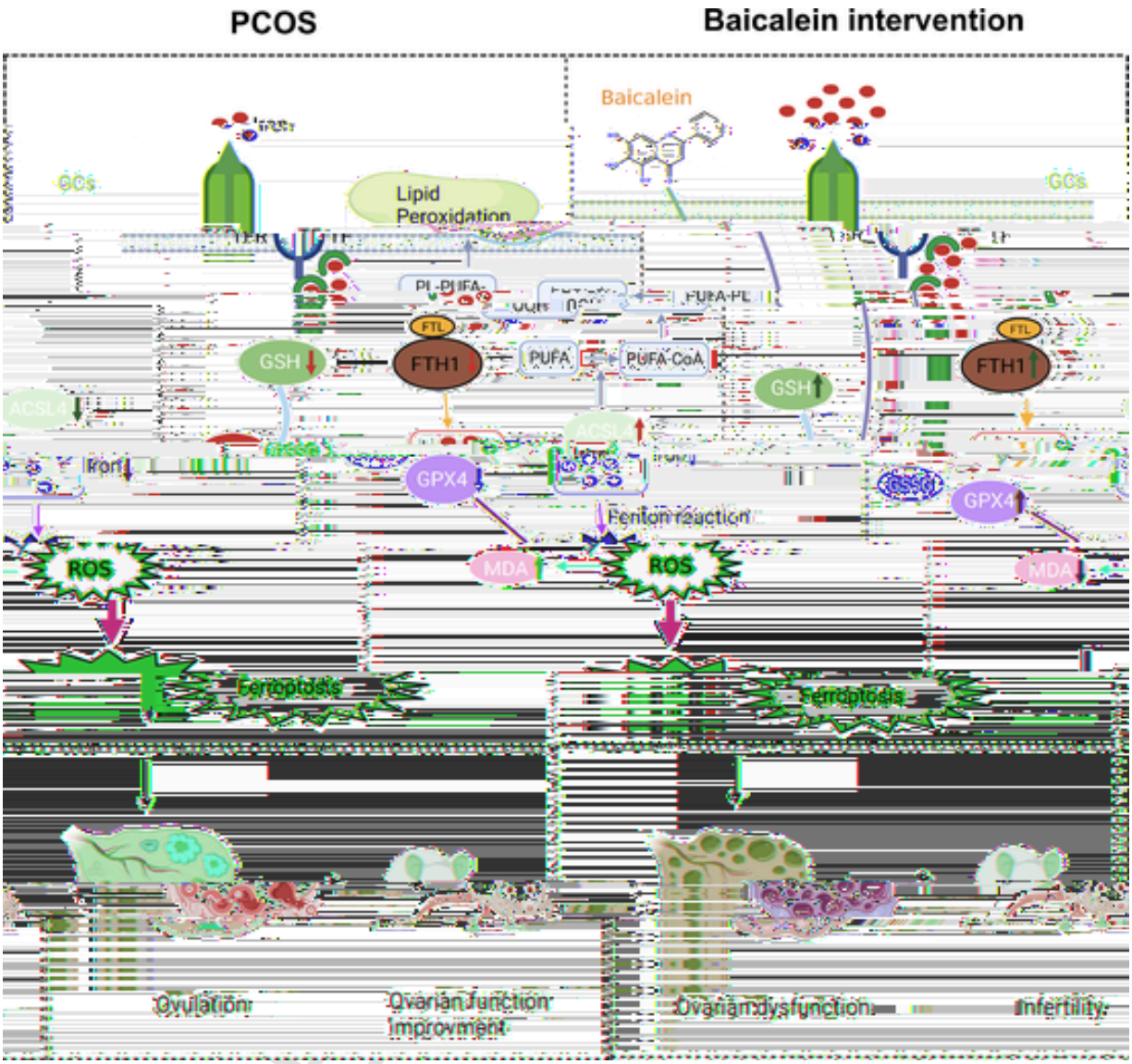

Fig. 8. A schematic depicting the mechanisms by which baicalein mediates antiferroptosis activity.
Abbreviations: GCs, Granulosa cells; TFR, Transferrin Receptor; TF, Transferrin; PUFA, Polyunsaturated fatty acid; PUFA-CoA, Polyunsaturated Fatty Acid-Coenzyme A; PUFA-PL, Polyunsaturated Fatty Acid-Phospholipid; PL-PUFA-OOH, Phospholipid Polyunsaturated Fatty Acid Hydroperoxide; GSSG, Glutathione disulfide.

Conclusions

In summary, our study investigated the mode of action of baicalein in PCOS, revealing novel insights that distinguish our research. The novelty of our study lies in uncovering the upregulation of ferroptosis in PCOS patients and suggesting that the therapeutic effect of baicalein may stem from its inhibition of this process. Ferroptosis, which acts as a regulator of oxidative stress pathways, adds a new dimension on PCOS pathogenesis and represents a potential treatment target. However, acknowledging the limitations of our study is crucial. We acknowledge that the animal model may not fully replicate the complexities of PCOS in humans and is influenced by various genetic and environmental factors. Additionally, while baicalein shows promise, more research needs to be done to find out how it works and establish its safety and efficacy in clinical settings. Moreover, we did not assess the pregnancy or live birth rates of the rats. To address these limitations, future research could incorporate larger sample sizes and diverse populations. During the course of our investigation, we encountered difficulties, mainly in the design and execution of animal experiments. To overcome these challenges, we carefully plan experimental designs and work with laboratory teams to demonstrate our commitment to methodological rigor and robustness in our study. Future investigations could focus on refining animal models to better mimic human PCOS and exploring additional interventions or combination therapies that may enhance treatment outcomes. Furthermore, clinical trials are necessary to determine baicalein's translational potential for PCOS in humans. These endeavors will help to better understand PCOS and develop effective treatments.

Access to Data

All of the data were in-house data only, and no use was made of paper mills. All authors agree that they are responsible for all aspects of the work and are guarantors of the integrity and accuracy of the work.

Funding

National Key Research and Development Program of China (No. 2016YFC1000100) partially supported this work, and Leading Talents

in the Construction Project of High Level Public Health Technical Talents in Beijing(No. 2022–1–003).

CRediT authorship contribution statement

Ying-ying Li: Writing – original draft. **Yi-qiu Peng:** Methodology. **Yu-xi Yang:** Methodology. **Ting-juan Shi:** Investigation. **Rui-xia Liu:** Writing – review & editing. **Ying-yi Luan:** Writing – review & editing. **Cheng-hong Yin:** Writing – review & editing.

Declaration of competing interest

The authors declare that they have no conflict of interest.

Supplementary materials

Supplementary material associated with this article can be found, in the online version, at doi:10.1016/j.phymed.2024.155423.

References

Azziz, R., Carmina, E., Chen, Z., Dunaif, A., Laven, J.S., Legro, R.S., Lizneva, D., Natterson-Horowtiz, B., Teede, H.J., Yildiz, B.O., 2016. Polycystic ovary syndrome. Nat. Rev. Dis. Primers. 2, 16057.

Bahri Khomami, M., Joham, A.E., Boyle, J.A., Piltonen, T., Silagy, M., Arora, C., Misso, M.L., Teede, H.J., Moran, L.J., 2019. Increased maternal pregnancy complications in polycystic ovary syndrome appear to be independent of obesity-A systematic review, meta-analysis, and meta-regression. Obes. Rev. 20 (5), 659–674.

Banik, K., Khatoon, E., Harsha, C., Rana, V., Parama, D., Thakur, K.K., Bishayee, A., Kunnumakkara, A.B., 2022. Wogonin and its analogs for the prevention and treatment of cancer: a systematic review. PhytOther Res. 36 (5), 1854–1888.

Beharier, O

Murri, M., Luque-Ramírez, M., Insenser, M., Ojeda-Ojeda, M., Escobar-Morreale, H.F., 2013. Circulating markers of oxidative stress and polycystic ovary syndrome (PCOS): a systematic review and meta-analysis. Hum. Reprod. Update 19 (3), 268–288.
Norman, R.J., Dewailly, D., Legro, R.S., Hickey, T.E., 2007. Polycystic ovary syndrome. Lancet. 370 (9588), 685–697.
Palierse, E., Hélary, C., Krafft, J.M., Génois, I., Masse, S., Laurent, G., Alvarez Echazu, M.I., Selmane, M., Casale, S., Valentin, L., Miche, A., Chan, B.C.L., Lau, C.B.S., Ip, M., Desimone, M.F., Coradin, T., Jolivalt, C., 2021. Baicalein-modified hydroxyapatite nanoparticles and coatings with antibacterial and antioxidant properties. Mater. Sci. Eng. C. Mater. Biol. Appl